Using Repeating Microearthquakes to Infer Medium Velocity Variations at Val d'Agri Area (Southern Italy)

Maha Adil, Mauro Palo, Aldo Zollo, Antonella Orefice, and Gianluca Dell'Elce

***Abstract*—We investigated the correlation between water level of Pertusillo artificial lake and both earthquake production and medium velocity changes in the Val d'Agri area (Southern Italy) estimated by Coda Wave Interferometry (CWI) applied to repeating microearthquakes. We analyzed a catalog of 3354 earthquakes occurred between 2019 and 2023. A total of 122 repeaters were identified using a multisensor clustering technique. We observed an annual periodicity in both medium velocity variation and lake water level, but the two series are time shifted of about 6 weeks. Adopting a pore pressure diffusion model, we estimated an effective hydraulic diffusivity of 0.1 m^2 /s. We found two spatial domains that respond differently to pore pressure changes: Within 5 km from the lake, positive pore pressure changes increase seismicity production, whereas, in the distance range 5–9 km, opposite pressure changes impact elastic properties and seismic velocities. Moreover, previous tomographic results suggest that these domains have a different lithology that results in a contrast in V_P/V_S and can promote fluid circulation. These findings suggest that seasonal water level fluctuations at the lake drive seismic activity and velocity changes in the area.**

***Index Terms*—Coda wave interferometry, hydraulic diffusivity, medium velocity variations, repeating earthquakes, Val d'Agri (Southern Italy).**

I. Introduction

THE correlation between human activities, particularly those connected to energy production, and the occurrence of earthquakes has garnered significant attention in recent years [1]. Anthropogenic activities such as hydraulic fracturing (fracking), geothermal energy production, and wastewater injection have been linked to the induction of seismic events, also known as induced earthquakes [2]. The mechanisms behind these induced earthquakes are complex and multifaceted, involving changes in the subsurface stress field due to fluid injection or extraction [1]. These activities can alter the stress balance within the Earth's crust, potentially triggering seismic events in regions where tectonic stress is already near a critical threshold [2], [3]. Significant attention has been paid to injection-induced seismicity in the USA after the 2011 Oklahoma earthquake (Mw 5.7), which has been linked to wastewater injection activities [4].

One of the primary mechanisms through which anthropogenic activities induce seismicity is through fluid injection, which leads to changes in pore pressure within the subsurface [5]. When fluids are injected into the Earth, they increase the pore pressure within the rock formations, which in turn reduces the effective normal stress on preexisting faults [5]. This reduction in stress can bring a fault closer to failure, thus triggering an earthquake [6]. Another important mechanism is the poro-elastic effect, where the injection or extraction of fluids causes deformation in the surrounding rock, altering the stress distribution and potentially inducing seismicity [3], [6]. These mechanisms are intrinsically linked to changes in the medium's elastic properties, including its seismic velocity [5]. As pore pressure increases or the poro-elastic response occurs, the stiffness of the rock can decrease, leading to a reduction in seismic wave velocities [6]. Such velocity reductions are also relevant to describe repeating earthquakes, which are often attributed to the interaction between velocity-weakening patches embedded within broader velocity-strengthening creeping regions [7]. Repeaters can thus be described as a response to the balance between seismic and aseismic slip, in addition to velocity-weakening and velocity-strengthening behavior, with pore pressure playing a role in modulating these regimes [7].

The Val d'Agri basin, located in the Southern Apennines of Italy, is an area of significant geological interest due to its active tectonic and seismotectonic settings. The basin lies in a region dominated by active thrusting and folding, processes that are typical of the Apennine mountain range. These tectonic features, combined with anthropogenic activities, contribute to a complex pattern of seismicity, characterized by both naturally occurring and induced earthquakes [8], [9], [10]. The basin hosts the Val d'Agri oil field, one of the largest onshore hydrocarbon production areas in Europe, where oil extraction activities and water re-injection are common. These energy production operations can influence the seismicity in the area [9], [11], [12]. In this region, seismicity is driven by both natural tectonic processes and anthropogenic activities, particularly those related to the Pertusillo artificial lake, the reservoir constructed in the

Received 23 June 2025; revised 1 October 2025 and 14 November 2025; accepted 9 December 2025. Date of publication 12 December 2025; date of current version 30 December 2025. The work of Maha Adil was supported by PhD fellowship funded by the National Operational Programme for Research and Innovation 20142020 (PON R&I), through ESF REACT-EU resources under Action IV.4 PhD programmes and research contracts on innovation-related topics and Action IV.5 PhD programmes on Green topics. *(Corresponding author: Mauro Palo.)*

Maha Adil, Mauro Palo, and Aldo Zollo are with the Department of Physics "Ettore Pancini", University of Naples Federico II, 80138 Naples, Italy (e-mail: mahaadil.mohamedaliebrahim@unina.it; mauro.palo@unina.it; aldo.zollo@unina.it).

Antonella Orefice and Gianluca Dell'Elce are with the Department of Geodynamic and Geophysical Monitoring, Eni S.p.A., 20124 Milan, Italy (e-mail: antonella.orefice@eni.com; gianluca.dellelce@eni.com).

Digital Object Identifier 10.1109/JSTARS.2025.3643734

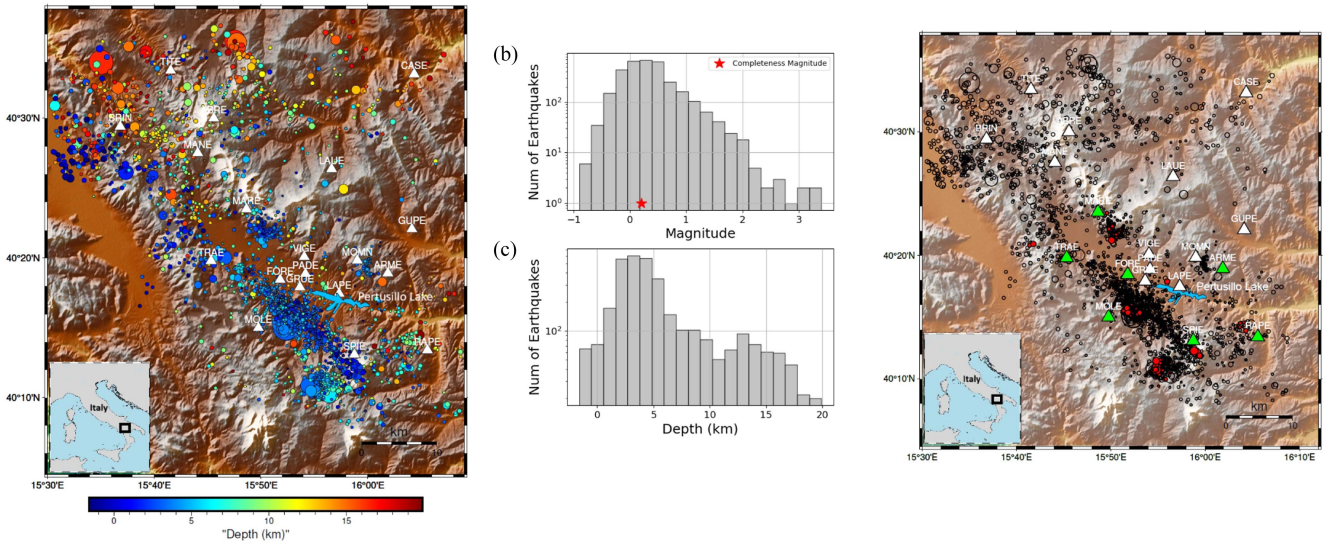

Fig. 1. (a) Dots show the epicenters of catalog earthquakes; size and color of the dots scale respectively with magnitude and depth. White triangles mark the location of ENI seismic stations. (b) Distribution of earthquake magnitudes together with the completeness magnitude estimated by the maximum curvature method.(c) Distribution of earthquake depths, displaying a bimodal pattern, indicating two distinct depth clusters. (d) Epicenters of repeaters (red dots) and the rest of the seismicity (black open circles). The symbols scale by magnitude. Green triangles mark the position of the seven receivers that detected the repeaters. White triangles mark the rest of the ENI seismic network.

1960s that plays a vital role in regional water management. This lake has been linked to reservoir-induced seismicity (RIS), where fluctuations in water levels can modify subsurface stress conditions, increasing pore pressure and affecting fault stability [9], [13]. The water level fluctuations in the Pertusillo reservoir have been closely associated with low-magnitude but persistent seismic activity. Studies have shown that as the water level rises or falls, there is a corresponding change in the stress regime within the subsurface, which can lead to seismic events [14], [15]. Ground motion data from the region suggests that the seismic response to the lake's operation is not instantaneous but evolves over time, with seismicity increasing during periods of water impoundment [14], [16].

In order to monitor both natural and induced seismicity, a comprehensive seismic network has been established in the Val d'Agri region. The network, owned and managed by ENI (the Italian multinational oil and gas company), includes both surface and borehole seismic stations, which provide high-resolution data on seismic events [17].

The goal of this study is to monitor medium velocity changes in the Val d'Agri region by coda wave interferometry of repeating earthquakes. Repeating earthquakes, or "repeaters," are seismic events that originate from nearly identical locations, that occur at different times, and have highly similar waveforms; these generally arise from the repeated rupture of the same or sub-parallel fault patches [18], [19], [20]. Repeaters can be considered natural, time-stable sources of seismic radiation, and any modifications over time of their waveform can therefore be attributed to changes in the elastic properties of the medium. Coda Wave Interferometry (CWI) exploits the property to infer medium velocity variations over time [21], [22], [23]. This study aims to enlighten the relationship between natural and anthropogenic activities and seismicity in the region, providing thus useful constraints for seismic monitoring and risk mitigation strategies.

II. Dataset

We analyzed a catalog of 3354 earthquakes nucleated in Val d'Agri between 2019 and 2023 as acquired by the 21 three-component stations of a local seismic network managed by ENI (Fig. 1(a)). The events have local magnitude M_L spanning in the range -0.9–3.4 with completeness magnitude equal to 0.2 [Fig. 1(b)]. The depths of the earthquakes show a bimodal distribution, with most events at depths around 5 km and another significant cluster at larger depths centered around 15 km [Fig. 1(c)].

As a preprocessing, the signals were band-pass frequency filtered in the range 1–20 Hz using a 4-pole Butterworth digital filter to mitigate microseismic and high-frequency noise. The first P-wave arrival times were automatically picked applying the FilterPicker algorithm [24] to the vertical component of the waveforms (see Fig. 2). In this way, we could identify the P arrival times for 21 080 waveforms.

III. Methodology

A. Identification of Repeating Earthquakes

Repeating earthquakes are generally identified by their high waveform similarity [18], [20], [21], [22], [25], [26], [27], [28]. Here we applied the first stage of the multichannel approach proposed by [19], who quantified the similarity between the waveforms by cross-correlation (CC) at different sensors. Following these authors, CC has been estimated on the vertical ground motion component and the waveforms were windowed by an 8-s boxcar beginning one second before the P onset.

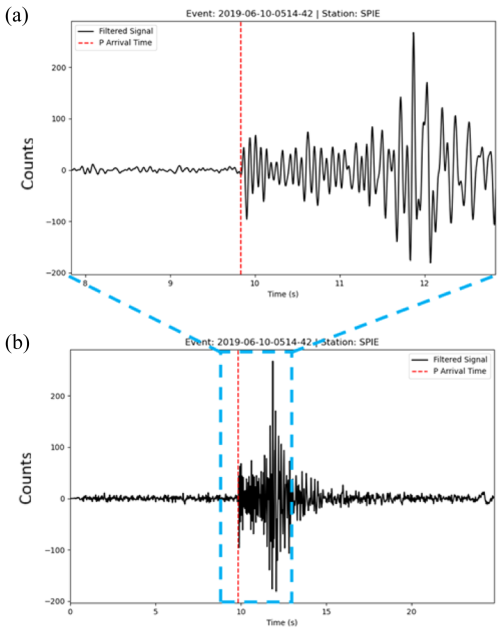

Fig. 2. (a) Zoomed-in view of the seismic trace recorded at station SPIE, highlighting the P arrival time marked by a vertical red dashed line. (b) Full seismic trace for the same event. The P arrival time was determined using the FilterPicker approach. For this detection, we used a sampling frequency of 200 Hz, corresponding to a time-delta dt of 0.005 s per sample. The FilterPicker parameters included a short-term filter window of 0.64 and a long-term window of 1.28 s. The detection threshold was set to 0.16, with primary and secondary threshold values of 10 and 5, respectively. This selection of parameters provided optimal conditions for detecting the P-wave arrival accurately.

The first P-wave arrival times were automatically picked by applying FilterPicker [24] to the vertical component of the waveforms. A CC value was finally estimated at each station for each pair of earthquakes of the catalog creating thus a CC matrix for each sensor. In each of these matrices, the elements with CC equal to or higher than 0.80 were identified; they are considered as produced by a pair of repeaters recorded at one sensor and adopted for detection of medium velocity variation. The total number of unique earthquakes producing high-CC elements at all stations was equal to 122; we will refer to this set of events as $\{R\}$. In Fig. 1(d), the earthquakes of $\{R\}$ are plotted as red dots.

B. Detecting Medium Velocity Variations

CWI determines changes in the travel times of coda waves, which are waves arriving after S waves and are scattered multiple times within the medium. CWI is sensitive to subtle changes in the velocity of the medium, as coda waves are highly influenced by the structure of the medium through which they propagate [29].

After the pioneering work of [21], several studies have utilized repeating earthquakes as a consistent source of seismic energy to infer changes in medium velocity [23], [28], [30], [31]. The core assumption is that for perfectly co-located earthquakes, any temporal variation in the coda waveforms observed at the same seismic station must be attributed to changes in the elastic properties of the medium. Variations in the medium velocity lead to stretching or compaction of the coda signal (that eventually manifests as time shifts in the waveforms) because coda waves are scattered, respectively, by a faster or slower medium [29], [32], [33].

The method measures in the coda (by maximizing CC) the time shift δt between the signals of a pair of repeaters occurring at different times. The relative change in medium velocity $\delta v/v$ is related to δt along the codas by [21]

$$\frac{\delta v}{v} = -\frac{\delta t}{t}. \tag{1}$$

Thus, linearly fitting in the $\delta t - t$ plane provides an estimate of the fractional velocity change.

To apply (1), we have first aligned the waveforms of a pair of repeaters on the P arrival times, and points of the $\delta t - t$ plane have been calculated aligning the waveforms of the pair of repeaters by CC in a time window $t_m = 1$s sliding of 0.2 s along the seismogram at each step; at each time, δt is the time lag that maximizes the CC. Points of $\delta t - t$ plane were then fit in the time range 2–8 s from the P onset; this time interval was selected to fit the part of the signals where coda waves dominate considering the mean theoretical S arrival resulting from the typical source-receiver distances and after visual inspection of several pairs of repeaters at different stations (see Fig. 3 for examples of linear fitting in the $\delta t - t$ plane).

Among all pairs of repeaters identified across the stations, we estimated $\delta v/v$ using those fulfilling two conditions: 1. the interrepeater time difference was equal or larger than 15 days; 2. the standard error in the linear regression in the $\delta t - t$ plane was less than 20% of the estimated velocity change ($\delta v/v$). Condition 1. aimed to select pairs with a sufficient time separation between events to capture meaningful changes in the medium over time; condition 2 guaranteed that the estimated $\delta v/v$ was robust and reliable. In this way, 139 pairs of repeaters were selected. All these pairs fulfilled the two conditions at a set of seven stations ($\{S\}$ here in after), which are displayed in Fig. 1(d) as green triangles.

For each station of $\{S\}$ and each repeater pair, we assigned $\delta v/v$ as estimated by fitting in $\delta t - t$ plane to the mean value of the occurrence times of the two repeaters. Moreover, we assigned an uncertainty to this value equal to the error in the linear fitting in the $\delta t - t$ plane. In Fig. 4 $\delta v/v$ so obtained at some stations is displayed; the gray horizontal line displays the time elapsed between the two repeaters.

Starting from the velocity variations of Fig. 4, the weekly rate of the velocity variations was estimated assuming a constant medium velocity variation between the times of the two repeaters of the pair and dividing $\delta v/v$ by the number of weeks elapsed between the two events. We considered then one week and identified the pairs spanning a time interval enclosing this week; the mean weekly medium velocity rate for this week was then computed by averaging the weekly $\delta v/v$ calculated over different pairs. The uncertainty on this mean weekly rate was fixed as the standard deviation of the $\delta v/v$ over the pairs. This process was repeated for all weeks of the time interval spanned between the earliest and the latest repeater and for each station. In this way, we retrieved a time series of the weekly medium

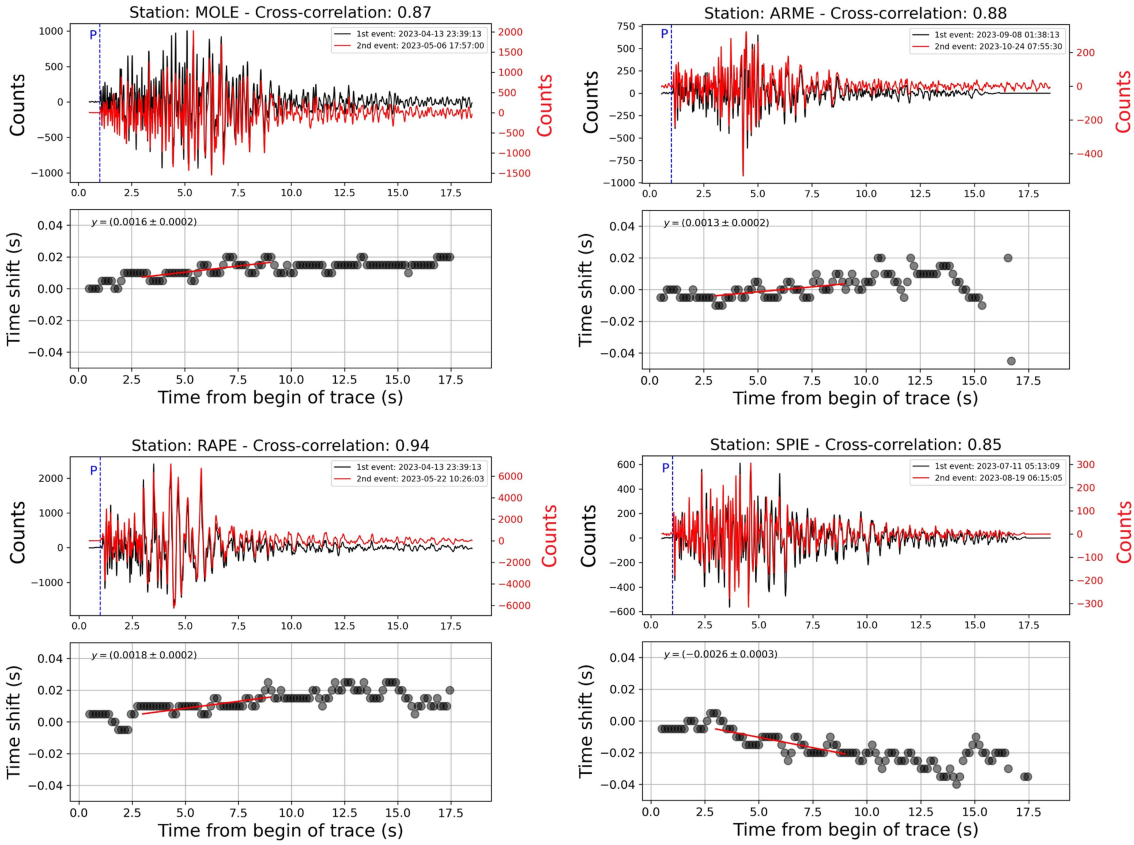

Fig. 3. Examples of pairs of repeaters at different stations. The corresponding time delay is estimated by aligning the two events of each pair and maximizing CC within a 1-s time window sliding by 0.2 s at each step. The red line in the $\delta t - t$ plane shows the best linear regression.

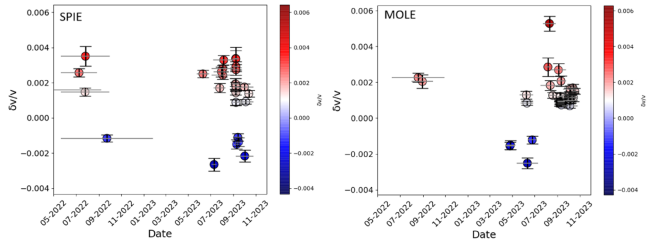

Fig. 4. Medium velocity variations $\delta v/v$ estimated from all pairs of repeaters at different stations. Each circle represents the $\delta v/v$ between the event pairs, estimated from the fitting line as described in (1). The color of the circles indicates whether the velocity increases (red) or decreases (blue), as shown in the color bar. The gray horizontal lines display the time between repeaters, with $\delta v/v$ values positioned at the mean time between the event pairs. The uncertainty represents the error of the linear fitting in the $\delta t - t$ plane.

velocity change for each station that we will indicate as $\delta v_i/v$, where i means the station index of the set $\{S\}$. Finally, $\delta v_i/v$ were averaged over the stations and $\delta v_m/v$ was defined.

Calculated $\delta v_i/v$ are displayed in Fig. 5(b) as colored dots, while $\delta v_m/v$ is shown as a dashed black line. In the same figure, the distribution of seismicity and the density of repeaters are displayed in the panel (a), while in the panel (c) the red curve shows the water level of the Pertusillo artificial lake and the blue line marks the rainfall.

$\delta v_i/v$ and consequently $\delta v_m/v$ show a quite regular pattern over time with a seasonal dependence of the medium velocity showing maxima in summer. The earthquake rate increases from April 2023; the highest rate occurs in July 2023 and is broadly synchronized with the peak in medium velocity increase. A 1-year periodicity is also visible in the time series of the water level in panel (c), although the maxima of this series are time-shifted with respect to the maxima $\delta v_i/v$ and earthquake rate.

IV. Discussion

The results of CWI on the repeaters described above show that the relative medium velocity variation appears to be modulated by a forcing factor with a periodicity close to one year. This result is visible at most stations, suggesting that the medium variations must involve a large volume of the area under study. On the other hand, the largest decrease of $\delta v/v$ is detected at the stations MOLE, RAPE (in April–May 2023), and station TRAE (in September–October 2023—Fig. 5), which are located well outside the volume of the earthquake cluster (Fig. 1(a)).

Two relative maxima of $\delta v/v$ (i.e., relative medium velocity increases) are visible in August 2022 and 2023. The latter $\delta v/v$ maximum is broadly synchronized with the earthquake rate peak. Minima in $\delta v/v$ appear broadly in April and September 2023, although we should consider that the timing of the series of $\delta v/v$ depends on the occurrence times of the repeaters and therefore cannot be considered as precise as the series of the water level and earthquake rate.

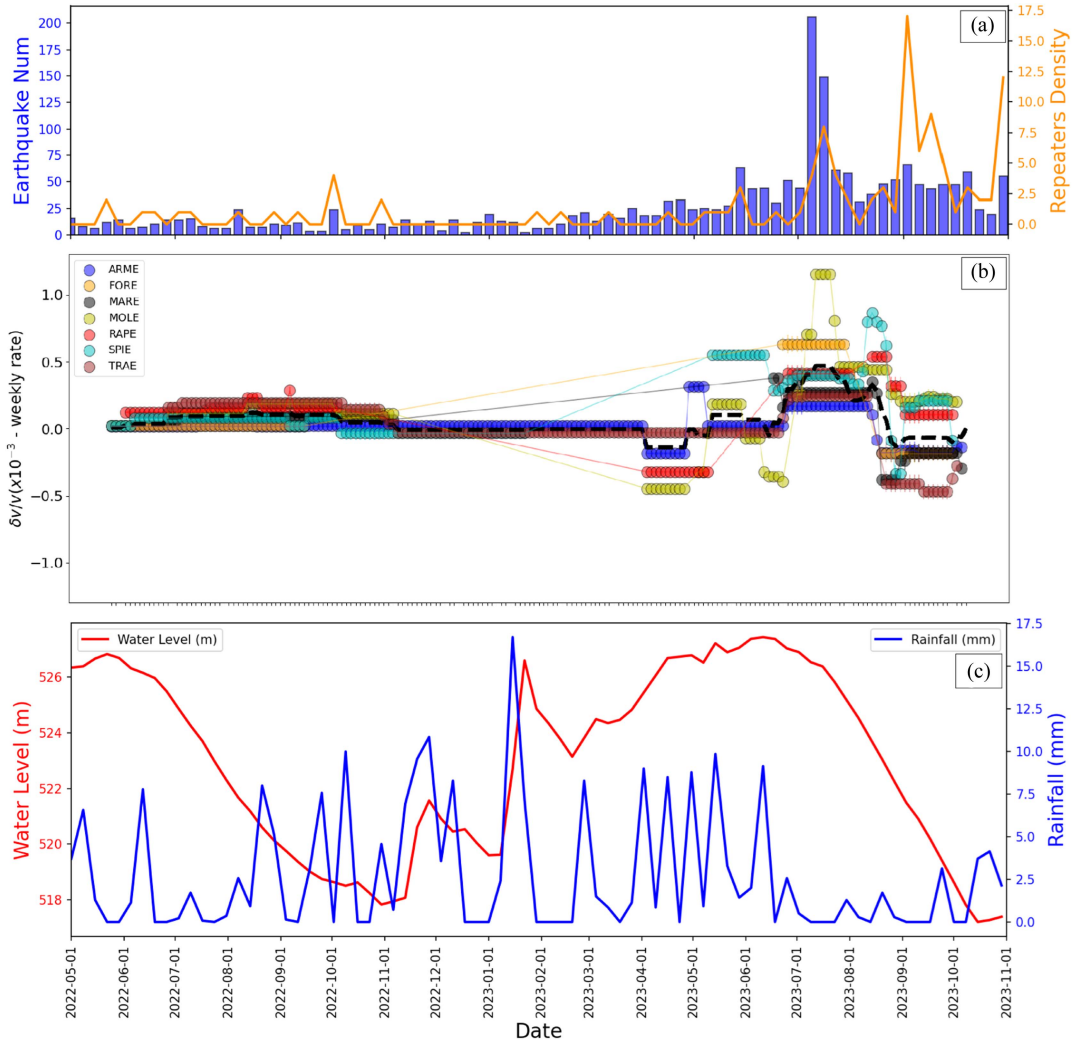

Fig. 5. (a) Weekly earthquake (blue bars) and repeater (orange line) rates. (b) Weekly velocity variations δv_i at all stations. The black dashed line displays δv_m, that is the mean δv over the stations. (c) Water level of Pertusillo artificial lake (red line) and rainfall level (blue line).

As already emphasized, the Pertusillo lake water level shows a 1-year periodicity, as well, but the maximum of this level is reached in June of the two years, that is, they are timely shifted with respect to the $\delta v/v$ maxima. In contrast, no clear temporal pattern is visible in the rainfall series, except for a larger mean rainfall in the second half of 2022 than in the same period of 2023 [Fig. 5(c)].

Previous studies [13], [15], [16] have argued that seismic activity in the Val d'Agri is primarily triggered by the water level oscillations of the Pertusillo lake. The same authors indicated as a triggering mechanism a local increase in pore pressure, which in turn would be originated by the oscillatory loading induced by water level oscillations. The authors in [13] demonstrated that the low-magnitude seismic activity correlates with the water level oscillations of the lake. They argued that the induced seismicity results from the loading and unloading associated with the seasonal water level changes, which lead to a pore pressure oscillation. Comparable fluid-driven mechanisms have also been reported in other tectonic settings where oscillatory pore pressure variations influence fault dynamics and earthquake recurrence [7], [34], indicating the general role of pore pressure changes in controlling seismic activity.

In line with previous works, we adopt here the straightforward framework that any medium velocity change is induced by water level oscillations of the Pertusillo lake, as well. Similarly, we assume that the pore pressure is spatially transferred by diffusion from the lake. This framework assumes a localized source of pressure variations (the lake) differently from cases in which the pore pressure variations may act simultaneously on large scales [35]. Under these conditions, we simulate the spatiotemporal propagation of the pore pressure wavefront induced by periodic water level oscillations. We estimate the maximum hydrostatic loading pressure variation from the water level changes as follows:

$$P_0 = (WL_{max} - \overline{WL})\rho g \tag{2}$$

where P_0 is the maximum variation of the pressure at the source, WL_{max} and $\overline{WL}$ are, respectively, the maximum and the mean water level, ρ is the water density (1000 kg/m^3), and g is the gravitational acceleration (9.81 m/s^2). For a spherical source

with radius a whose pressure varies harmonically with angular frequency ω and propagates by diffusion, the spatiotemporal pore pressure pattern at distance r from the source and time t is [36]

$$P(r,t) = P_0 \frac{a}{r} e^{\left[(a-r)\sqrt{\frac{\omega}{2D}}\right]} e^{i\left[(r-a)\sqrt{\frac{\omega}{2D}} - \omega t - \phi\right]} \quad (3)$$

where D is the hydraulic diffusivity and ϕ is a phase shift to account for the fact that the water level oscillations do not start from zero in the observed time interval. We fix ϕ by fitting the water level time series with a sin function and select the angular phase that maximizes the overlap between the two functions.

Equation (3) contains an oscillatory term, which depends on the harmonic pressure oscillations at the source and on the effects of diffusive propagation ($e^{i[(r-a)\sqrt{\frac{\omega}{2D}} - \omega t - \phi]}$) and a spatial attenuation factor ($\frac{a}{r} e^{[(a-r)\sqrt{\frac{\omega}{2D}}]}$).

We model the effects of the water level oscillations as a result of a harmonic pressure change within a sphere of radius of 2000 m, which is selected as an effective radius considering the surface of the lake (approximately 7 km by 2 km). The effective radius is chosen to approximately equal the area of a circle with this radius with the area of a rectangle that has the sizes of the lake.

We first estimate the value of the hydraulic diffusivity in the following way. We simulate the pore pressure over time using (3) fixing the distance r to r_0 =5 km, which is the mean distance between the lake and most earthquake epicentres (see Fig. 1). Then, we let D vary over four orders of magnitude, that is between 0.01m^2 /s and 10 m^2/s (i.e., the typical range in the Earth's crust [37]) and fix the best estimate of D maximizing the CC between $P(t, r = r_0)$ and the time series of the earthquake rate. We implicitly assume that earthquake production is promoted by a positive pore pressure wavefront originating by lake water level oscillations and propagating by diffusion from the lake outward. In this way, we find the best overlap between earthquake rate and positive pore pressure for $D_0 = 0.1$ m^2/s.

Fig. 6(a) and (b) show, respectively, the CC between the observed water level oscillations and 1. earthquake rate and 2. medium velocity variations. In both cases, the maximum overlap between the curves is obtained for a time shift of 6 weeks, which is a measure of the time needed by the pore pressure perturbation to propagate towards the medium; we indicate this time as t_0. Consistently, [10] found a time shift of about 40 days between the first loading phase of the Pertusillo lake and V_p/V_S trends.

However, we find an increase in the medium velocity broadly in correspondence with the earthquake rate maximum. This is in contradiction with the hypothesis that earthquakes are mostly triggered by diffusion of positive pore pressure promoting the fault slip, whereas theory predicts that a pore pressure increase implies an increase of the volume of fluid-filled cracks and therefore a decrease of the seismic velocity of the medium.

CWI indicates an overall velocity change detected at several stations covering a large volume of Val d'Agri (interstation distances in the order of 10 km). This means that the velocity anomaly cannot be easily localized and is possibly spatially diffused. However, CWI also shows that at stations MOLE, TRAE, RAPE, and SPIE, the medium velocity changes are relatively high (see Fig. 5(b)). Interestingly, these stations are located outside the main cluster of earthquakes, as visible from Fig. 7, where we have shown the $\delta v/v$ for each earthquake pair-station combination, drawing each ray as a straight line connecting source and station whose color scales by velocity change. We note that the largest velocity variations are detected

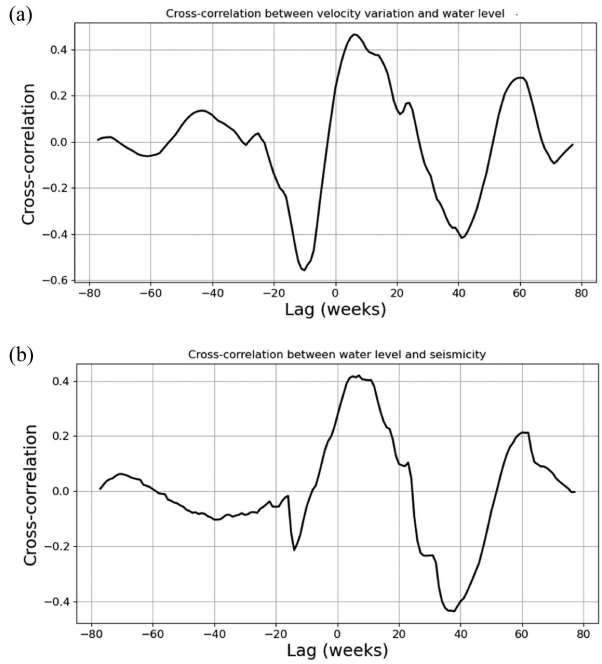

Fig. 6. (a) CC between water level oscillations and medium velocity variations. It shows a peak correlation of 0.47 with a time delay of 6 weeks. (b) CC between water level oscillations and earthquake rate. CC maximum is 0.42 for a time shift of 6 weeks.

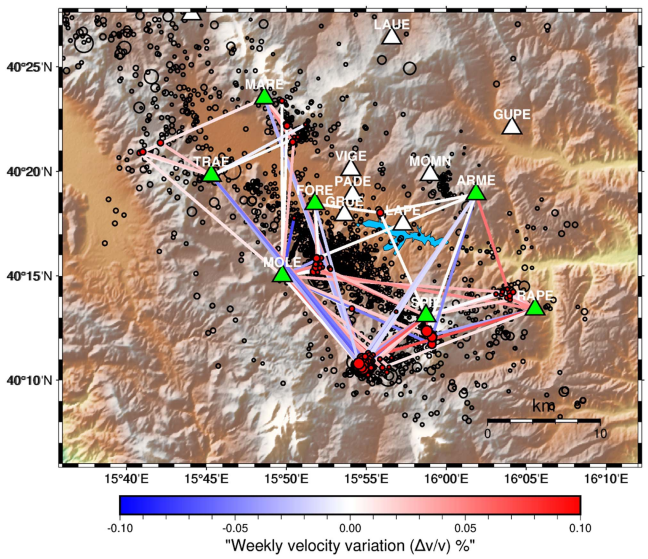

Fig. 7. $\delta v/v$ for each combination of repeater pair - station. The straight lines connect repeater epicenters (mean position of the pair) with the station and broadly represent the medium sampled by the seismic ray. The color of the ray scales with $\delta v/v$. The largest values of velocity variations are detected for rays that do not cross the main earthquake cluster.

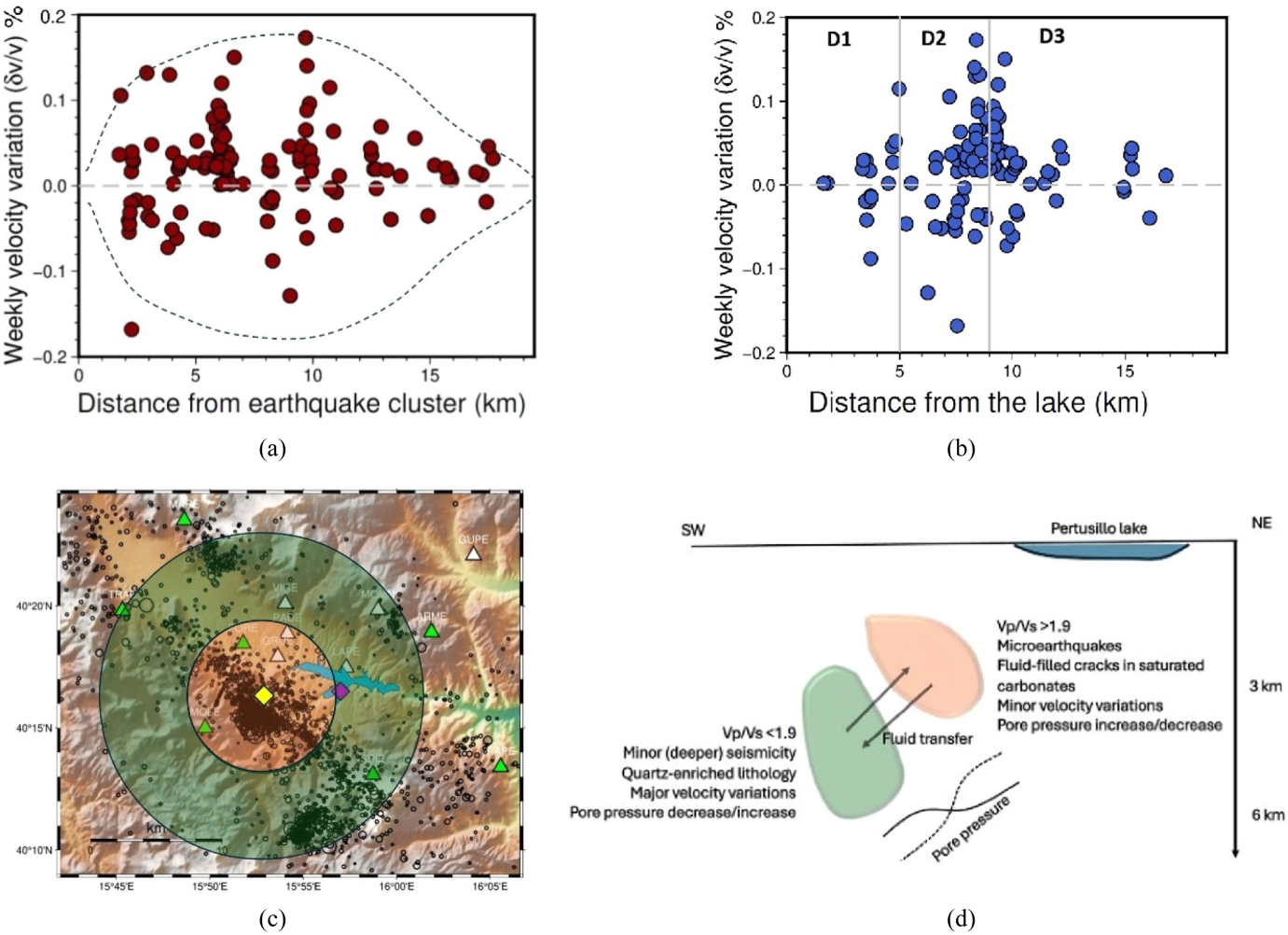

Fig. 8. (a) $\delta v/v$ as a function of the distance between the rays connecting the repeater pair and the station and the centroid of the main earthquake cluster. The dotted lines are specular and roughly draw the envelopes of the points. The largest values of $\delta v/v$ (in absolute value) are detected at distances between 5 km and 10 km from the earthquake cluster centroid (yellow diamond in panel b); $\delta v/v$ is on average relatively small for distances lower than about 5 km, i.e., for rays that cross the main earthquake cluster. (b) Sketch of spatial pattern of $\delta v/v$. In the volume of the main earthquake cluster (inner yellow circle), $\delta v/v$ is mostly lower than in the surrounding volume (outer green circle). The yellow diamond marks the earthquake cluster centroid. (c) $\delta v/v$ as a function of the distance from the Pertusillo lake (magenta diamond in panel b). (d) Sketch of the relatively low- and high-V_P/V_S volumes. The two volumes have different lithology, which affects the medium elastic properties and the capability to generate earthquakes.

for rays that do not cross the main earthquake cluster. In particular, rays that connect ARME to repeaters that nucleated in the center of the main earthquake cluster show very low values of $\delta v/v$, while rays connecting the same station to repeaters outside the center of the main earthquake cluster show larger values of $\delta v/v$.

In Fig. 8(a) we plot $\delta v/v$ as a function of the distance between the middle point of the ray connecting station and repeater pair and a reference point broadly fixed at the center of the main earthquake cluster [yellow diamond in Fig. 8(b)]. This distance thus represents a characteristic distance between the medium sampled by the ray and the main earthquake cluster. We find that at small distances from the earthquake cluster centroid ($<$ 5 km) $\delta v/v$ is on average smaller (in absolute value) than at distances in the range of 5–10 km from the cluster centroid. One negative outlier appears about 2 km from the centroid, but the corresponding ray samples actually a volume at the western border of the earthquake cluster (short ray from MOLE in Fig. 7). The results thus suggest the existence of two domains: A low-$\delta v/v$ volume spatially matching the main earthquake cluster, and a high-$\delta v/v$ volume located at larger distances from the lake [Fig. 8(b)]. In the panel (c) of the same figure, $\delta v/v$ is plotted as a function of the distance from the Pertusillo lake. The figure shows that high velocity variations (in absolute values) are detected in the range of distances from the lake of 6–10 km, while at shorter distances $\delta v/v$ values are lower on average.

To better locate the volume primarily affected by changes in the medium velocity, we apply (3) fixing $D = D_0$ and t=t_0. Fig. 9 shows the profile of $P(r, t = t_0, D = D_0)$ (red line). Only solutions for $r > a$ are physically meaningful; so the plot starts from r =2000m, and the values on the x-axis should be considered as the distances from the edge of the 2 km-radius sphere that we have assumed as the pressure source. We find positive pore pressures for distances (from the source boundary) smaller than about 2.8 km; in this distance range, P assumes values up to 40 kPa. At distances in the range 2.8–5.8 km, we

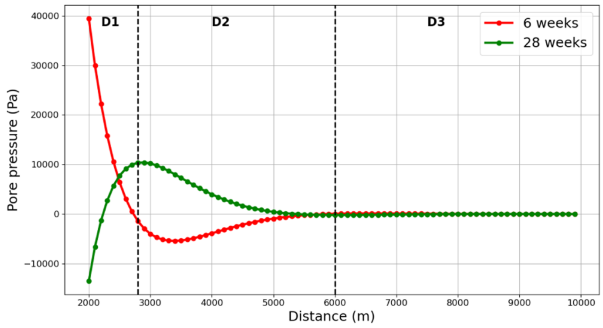

Fig. 9. Pore pressure as a function of distance. The red markers represent pore pressure calculated with fixed values of D_0 and t_0 (6 weeks), while the green markers represent pore pressure calculated with fixed values of D_0 and ($t = t_1$) (28 weeks).

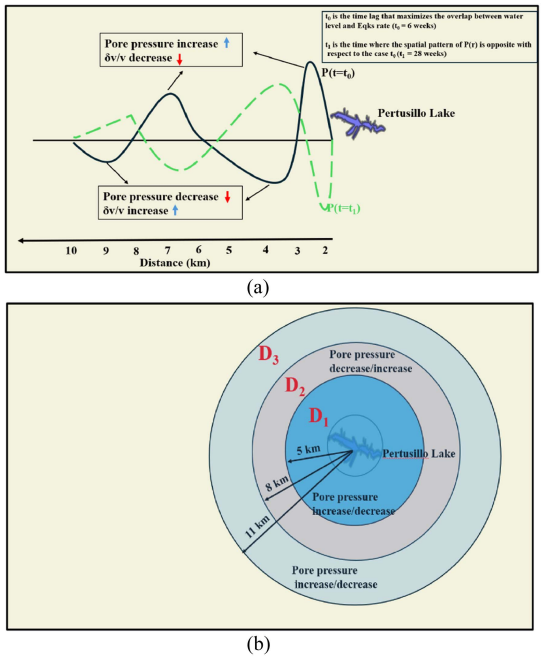

Fig. 10. (a) Sketch of pore pressure P(r) profiles at t= t_0 (solid line) and t= t_1 (dashed line), corresponding to time delays of 6 and 28 weeks, respectively. Positive pore pressure (red) supports earthquake triggering, while negative (green) may induce medium velocity increase. (b) Three zones around Pertusillo Lake D_1 (up to 2.8 km from the source boundary), where pore pressure increases may trigger earthquakes; D_2 (3–6 km) where pore pressure affects medium velocity; and D_3 (> 6 km) where the changes do not significantly affect either earthquake production or medium velocity changes.

find negative pore pressures up to about 5.5 kPa. At distances larger than about 6 km (and up to about 9 km) the model predicts again a pore pressure increase, but with very low amplitude (in the order of 0.1 kPa). In Fig. 10, we label these three domains as D_1, D_2, and D_3. As visible from Fig. 8(c), the largest medium velocity variations occur in D_2, which thus largely overlaps with the high-$\delta v/v$ volume, while D_1 broadly matches spatially the low-$\delta v/v$ volume.

The typical pore pressures that can trigger an earthquake are on the order of 10–100 kPa or more [37]. Our model predicts that D_1 can experience pore pressure increases compatible with the earthquake triggering, and thus at least a part of the earthquakes that occur in a radius of 5 km from the lake could be triggered by water level oscillations. Differently, volumes of D_2 could be the cause of increases in $\delta v/v$. This would be reasonable considering the typical interreceiver distances and the size of the volume crossed by the interrepeater seismic rays [both in the order of 10 km—see Fig. 1(d)]. Pore pressure variations predicted in D_3 are too low to affect both earthquake production and medium velocity.

From Fig. 5(b), we can see that the distance between the first $\delta v/v$ maximum (August 2022) and minimum (April 2023) is about 28 weeks (t_1). Simulating $P(r, t = t_1, D = D_0)$, that is, looking at the spatial pressure profile after $t = t_1$, we find positive pore pressure variations in D_2 in the order of 10 kPa (see green line of Fig. 9); this pattern can explain the observed medium velocity decrease after $t = t_1$. In contrast, this simulation shows both positive and negative pore pressure variations in D_1 (again of the order of 10 kPa), which could result in a net unaffected earthquake production, in line with the nearly stationary earthquake rate observed in correspondence of the $\delta v/v$ minima [Fig. 5(b)].

The authors in[10] mapped the tomography of the Val d'Agri area using earthquakes detected during a temporary measurement campaign. Interestingly, they found a volume with high V_P/V_S (1.9-2.1) at depths of about 3 km that encircles the Val d'Agri basin. Moreover, they found that this volume spatially matched very well the hypocentres of the main cluster of microearthquakes, which appeared to be nearly exclusively located in this volume. The authors also highlighted that such a high-V_P/V_S volume was bordered south-west and partially at larger depths with a volume in which relatively low V_P/V_S values were found (1.8–1.9); in this latter volume a secondary cluster of microearthquakes nucleated at depths 3–6 km (see Figs. 3– 4 in [10]). The authors also found a different time variation of V_P/V_S for stations located above the earthquake cluster and outside it. All these results indicate the existence of two volumes with a sharp contrast in rheology and/or lithology, one of which spatially matches the volume where most microearthquakes nucleate. Specifically, the authors associated the high-V_P/V_S volume with fractured and fluid-saturated carbonates prone to generate earthquakes, whereas they modeled the neighboring volume with lower V_P/V_S as a quartz-enriched lithology and/or a less developed system of cracks.

Based on this scheme, our results indicate that the (relatively) low-V_P/V_S volume is more sensitive to medium velocity variations, while the high-V_P/V_S volume is more prone to earthquake generation. Moreover, our model implies that the two volumes experience different pore pressure variations induced by lake water oscillations, thus creating a pore pressure gradient between the volumes. As also supposed in [10], we imagine that the two volumes can exchange fluids, potentially promoted by the contrast in rheology that could enhance the pore pressure gradient. In this scheme, the decrease in velocity detected in April 2023 can be explained by a pore pressure increase in the low-V_P/V_S volume. The subsequent medium velocity increase would be again experienced by the low-V_P/V_S volume and induced by a pore pressure decrease. At the same time, the increase in earthquake production in the high-V_P/V_S volume

would be due to a pore pressure increase in this volume, potentially promoted by the contrast in rheology (from a less cracked to a more cracked medium) and induced by fluids migrating from the low-V_P/V_S volume. Differently, the medium velocity increase in August 2022 is not followed by a relevant increase in earthquake production. In this case, the increase in $\delta v/v$ is smaller than in 2023; we can imagine that in this case the pore pressure increase is not large enough to enhance the number of triggered earthquakes, possibly due to time-dependent local stress conditions of the fault network and/or small-scale stress redistribution that our model does not consider. Nevertheless, the lower values of $\delta v/v$ in 2022 could be at least partially also influenced by the lower earthquake rate in this period that, in turn, leads to a lower density of the rays and thus to a coarser spatial sampling of the medium.

In Fig. 8(b) and (d), we have sketched the two volumes. The high-V_P/V_S volume has a radius of about 5 km and is centered on the area where most microearthquakes nucleate. It is characterized by a highly fractured fluid-rich carbonate medium. Despite that, minor medium velocity changes are detected in this volume. The high-V_P/V_S volume is bordered by the relatively low-V_P/V_S volume, which is highly sensitive to medium velocity variations, possibly indicating a large variation in fluid content. It can be quartz-enriched and/or less cracked than the high-V_P/V_S volume. Seismicity production in the low-V_P/V_S volume is secondary and limited to a minor earthquake cluster at depths of 3-6 km south-west of the main cluster in the high-V_P/V_S volume. The two volumes experience different trends of the pore pressure variations, ultimately connected to the lake water level oscillations.

V. Conclusion

We have found a correlation between the water level of the Pertusillo artificial lake and both earthquake production and medium velocity change inferred by coda wave interferometry applied to repeaters detected in the Val d'Agri (Southern Italy). We impute this correlation to a diffusive propagation of an oscillatory pore pressure induced by water level oscillations through a poro-elastic mechanism. We have estimated an effective hydraulic diffusivity in the area of about 0.1 m^2 /s. Moreover, we have identified two spatial domains in which the pore pressure propagation has opposite effects: at short distances from the lake (up to about 5 km from the lake center, D_1), the pore pressure variations have the same sign as those at the source, while at larger distances (up to about 8 km, D_2), they have opposite signs. This implies that D_1 is sensitive to an increase in earthquake production when the pore pressure wavefront has a positive sign, while D_2 is sensitive to changes in the pore pressure that modify the elastic properties of the medium and eventually the seismic velocity.

Based on results from the literature, we have estimated that D_1 and D_2 are distinguished in lithology producing a contrast in V_P/V_S. D_1 is a volume with a radius of about 5 km of cracked and fluid-rich saturated carbonates with high V_P/V_S and prone to earthquake production; D_2 surrounds the volume of D_1 at larger depths, possibly has a quartz-enriched lithology, and experiences large changes in the medium velocity. This sharp contrast in lithology could enhance the difference in pore pressure experienced by the two volumes, which could react differently to the diffusing pore pressure wave.

In conclusion, our work indicates that the microseismicity and medium properties in the Val d'Agri are mainly driven by the Pertusillo lake water level, which shows a periodicity of about one year. In that sense, a future extended study of the effects of these oscillations on seismicity and medium velocity should consider a longer time period of observations than 1.5 years analyzed in this work.

In addition, although the spatiotemporal pattern of the modeled pore pressure fluctuations can fit the main observations of velocity changes and earthquake production, it fails in reproducing small-scale behavior such as the time-variable earthquake rate, which can be affected by local stress redistribution and fluid migration so far neglected in the modeling. An extension of our approach should also account for these small-scale interactions that may relevantly affect the triggering of the earthquakes.

Acknowledgment

The authors would like to thank Tony Alfredo Stabile for providing the water level data of Pertusillo Lake. The complete time history is available upon request (tonyalfredo.stabile@cnr.it), and day-by-day data can be downloaded from http://www.adb.basilicata.it/adb/risorseidriche/dispoidriche/sceglidatidighe.asp.

The catalog of seismic events and waveforms used in this study must be requested directly from Eni by contacting coauthors Antonella Orefice (Antonella.Orefice@eni.com) or Gianluca Dell'Elce (Gianluca.Dellelce@eni.com).

P-wave arrival times were automatically picked using FilterPicker [24], and maps were generated using the PyGMT library [38].

References

[1] W. L. Ellsworth, "Injection-induced earthquakes," vol. 341, no. 6142, 2013, Art. no. 1225942.

[2] National Research Council, *Induced Seismicity Potential in Energy Technologies*. Washington, D.C.: National Academies Press, 2013.

[3] M. Palo, E. Ogliari, and M. Sakwa, "Spatial pattern of the seismicity induced by geothermal operations at the geysers (california) inferred by unsupervised machine learning," *IEEE Trans. Geosci. Remote Sens.*, vol. 62, 2024, Art. no. 5905813.

[4] K. M. Keranen, H. M. Savage, G. A. Abers, and E. S. Cochran, "Potentially induced earthquakes in oklahoma, USA: Links between wastewater injection and the 2011 mw 5.7 earthquake sequence," *Geology*, vol. 41, no. 6, pp. 699–702, 2013.

[5] P. Segall, "Earthquakes triggered by fluid extraction," *Geology*, vol. 17, no. 10, pp. 942–946, 1989.

[6] S. A. Shapiro, C. Dinske, C. Langenbruch, and F. Wenzel, "Seismogenic index and magnitude probability of earthquakes induced during reservoir fluid stimulations," *Leading Edge (Tulsa, OK)*, vol. 29, pp. 304–309, 2010.

[7] M. Toker, "Symptomatic discretization of small earthquake clusters reveals seismic coupling to 2017 bodrum earthquake (mw 6.6) in the gulf of gökova (sw corner of Turkey): Viscous-compliant seismogenesis over back-arc setting," *J. Afr. Earth Sci.*, vol. 177, 2021, Art. no. 104156.

[8] L. Benedetti, P. Tapponnier, G. C. King, B. Meyer, and I. Manighetti, "Growth folding and active thrusting in the montello region, veneto, northern Italy," *J. Geophys. Res.: Solid Earth*, vol. 105, no. B1, pp. 739–766, 2000.

[9] L. Valoroso et al., "Active faults and induced seismicity in the Val d'Agri area (southern apennines, Italy)," *Geophysical J. Int.*, vol. 178, no. 1, pp. 488–502, 2009.
[10] L. Valoroso, L. Improta, P. De Gori, and C. Chiarabba, "Upper crustal structure, seismicity and pore pressure variations in an extensional seismic belt through 3-d and 4-d vp and vp/vs models: The example of the Val d'Agri area (Southern Italy)," *J. Geophysical Research: Solid Earth*, vol. 116, no. B7, 2011, Art. no. B07303.
[11] L. Improta, L. Valoroso, D. Piccinini, and C. Chiarabba, "A detailed analysis of wastewater-induced seismicity in the Val d'Agri oil field (Italy)," *Geophysical Res. Lett.*, vol. 42, no. 8, pp. 2682–2690, 2015.
[12] B. H. Hager et al., "A process-based approach to understanding and managing triggered seismicity," *Nature*, vol. 595, no. 7869, pp. 684–689, 2021.
[13] Stabile, A. Giocoli, V. Lapenna, A. Perrone, S. Piscitelli, and L. Telesca, "Evidence of low-magnitude continued reservoir-induced seismicity associated with the pertusillo artificial lake (Southern Italy)," *Bull. Seismological Soc. America*, vol. 104, no. 4, pp. 1820–1828, 2014.
[14] T. Stabile, A. Giocoli, A. Perrone, S. Piscitelli, L. Telesca, and V. Lapenna, "Relationship between seismicity and water level of the pertusillo reservoir (Southern Italy)," in *Bollettino diGeofisicaTeoricaed Applicata*, no. 4, 2015, pp. 505–517.
[15] A. P. Rinaldi, L. Improta, S. Hainzl, F. Catalli, L. Urpi, and S. Wiemer, "Combined approach of poroelastic and earthquake nucleation applied to the reservoir-induced seismic activity in the Val d'Agri area, Italy," *J. Rock Mechan. Geotechnical Eng.*, vol. 12, no. 4, pp. 802–810, 2020.
[16] M. Picozzi, V. Serlenga, and T. A. Stabile, "Spatio-temporal evolution of ground motion intensity caused by reservoir-induced seismicity at the pertusillo artificial lake (Southern Italy)," *Front. Earth Sci.*, vol. 10, 2022, Art. no. 1048196.
[17] T. A. Stabile et al., "The insieme seismic network: A research infrastructure for studying induced seismicity in the high agri valley (Southern Italy)," *Earth Syst. Sci. Data*, vol. 12, no. 1, pp. 519–538, 2020.
[18] N. Uchida and R. Bürgmann, "Repeating earthquakes," *Annu. Rev. Earth Planet. Sci.*, vol. 47, pp. 305–332, 2019.
[19] M. Palo, M. Picozzi, G. De Landro, and A. Zollo, "Microseismicity clustering and mechanic properties reveal fault segmentation in Southern Italy," *Tectonophysics*, vol. 856, 2023, Art. no. 229849.
[20] M. Palo, F. S. di Uccio, M. Picozzi, and G. Festa, "An enhanced catalog of repeating earthquakes on the 1980 irpinia fault system, Southern Italy," *Geosciences*, vol. 14, no. 1, p. 8, 2023, Art. no. 8, doi: 10.3390/geosciences14010008.
[21] G. Poupinet, W. L. Ellsworth, and J. Frechet, "Monitoring velocity variations in the crust using earthquake doublets: An application to the calaveras fault, california (USA)," *J. Geophysical Res.*, vol. 89, pp. 5719–5731, 1984.
[22] R. M. Nadeau and L. R. Johnson, "Seismological studies at parkfield vi: Moment release rates and estimates of source parameters for small repeating earthquakes," *Bull. Seismological Soc. America*, vol. 88, no. 3, pp. 790–814, 1998.
[23] M. Palo, V. Cascone, M. Adil, and A. Zollo, "Repeating long-period earthquakes at shishaldin volcano (alaska): Insights into the source mechanism and relationship to volcano dynamics," *J. Geophysical Res.: Solid Earth*, vol. 130, no. 8, 2025, Art. no. e2024JB030480.
[24] A. Lomax, C. Satriano, and M. Vassallo, "Automatic picker developments and optimization: Filterpicker—a robust, broadband picker for real-time seismic monitoring and earthquake early warning," *Seismological Res. Lett.*, vol. 83, no. 3, pp. 531–540, 2012.
[25] J. Vidale, W. EIIsworth, A. Cole, and C. Marone, "Variations in rupture process with recurrence interval in a repeated small earthquake," *Nature*, vol. 368, no. 6472, pp. 624–626, 1994.
[26] R. M. Nadeau, W. Foxall, and T. McEvilly, "Clustering and periodic recurrence of microearthquakes on the san andreas fault at parkfield, california," *Science*, vol. 267, no. 5197, pp. 503–507, 1995.
[27] A. M. Rubin, D. Gillard, and J.-L. Got, "Streaks of microearthquakes along creeping faults," *Nature*, vol. 400, no. 6745, pp. 635–641, 1999.
[28] D. P. Schaff and G. C. Beroza, "Coseismic and postseismic velocity changes measured by repeating earthquakes," *J. Geophysical Research: Solid Earth*, vol. 109, Oct. 2004, Art. no. B10302.
[29] R. Snieder, A. Grêt, H. Douma, and J. Scales, "Coda wave interferometry for estimating nonlinear behavior in seismic velocity," *Science*, vol. 295, no. 5563, pp. 2253–2255, 2002.
[30] A. Ratdomopurbo and G. Poupinet, "Monitoring a temporal change of seismic velocity in a volcano: Application to the 1992 eruption of mt. merapi (Indonesia)," *Geophysical Res. Lett.*, vol. 22, no. 7, pp. 775–778, 1995.
[31] D. P. Schaff, G. C. Beroza, and B. E. Shaw, "Postseismic response of repeating aftershocks," *Geophysical Res. Lett.*, vol. 25, no. 24, pp. 4549–4552, 1998.
[32] A. Grêt, R. Snieder, R. C. Aster, and P. R. Kyle, "Monitoring rapid temporal change in a volcano with coda wave interferometry," *Geophysical Res. Lett.*, vol. 32, no. 6, 2005, Art. no. L06304.
[33] R. Snieder, "The theory of coda wave interferometry," *Pure Appl. Geophys.*, vol. 163, pp. 455–473, 2006.
[34] M. Toker, E. Yavuz, and E. Balkan, "Focal mechanisms and bouguer-gravity anomalies of the 2025 earthquake cluster in the santorini-amorgos region (southern aegean sea, Greece): Evidence for shallow extensional magmatism," *J. Seismol.*, vol. 29, pp. 1–19, 2025.
[35] T. Clements and M. A. Denolle, "Tracking groundwater levels using the ambient seismic field," *Geophysical Res. Lett.*, vol. 45, no. 13, pp. 6459–6465, 2018.
[36] S. A. Shapiro, E. Huenges, and G. Borm, "Estimating the crust permeability from fluid-injection-induced seismic emission at the ktb site," *Geophysical J. Int.*, vol. 131, no. 2, pp. F15–F18, 1997.
[37] P. Talwani and S. Acree, "Pore pressure diffusion and the mechanism of reservoir-induced seismicity," in *Earthquake Prediction*, vol. 122, pp. 947–965, 1985.
[38] L. Uieda et al., "Pygmt: A python interface for the generic mapping tools," *Zenodo*, Feb. 2021, doi: 10.5281/zenodo.4522136.

Maha Adil received the M.Sc. degree in physics from Al-Neelain University, Khartoum, Sudan, in 2019, and the Ph.D. degree in physics from the University of Naples "Federico II," Naples, Italy, in 2025.

Since 2022, she has been working on unsupervised machine-learning techniques for the identification of repeating earthquakes and has applied coda wave interferometry to study medium velocity variations in tectonic and volcanic regions, with the aim of detecting spatiotemporal changes associated with stress accumulation and fault system dynamics.

Mauro Palo received the Ph.D. degree in physics from the University of Salerno, Italy, in 2008.

He is an Associate Professor with the Department of Physics, University of Naples "Federico II," Naples, Italy. His research focuses on the study of microseismicity clusters in volcanic, tectonic, and industrial or geothermal settings, with the goal of characterizing medium and source properties and their correlation with spatiotemporal variations in the stress field. He also works on modeling the source of volcanic seismicity and tracking rupture fronts during large earthquakes using advanced seismological techniques. He specializes in numerical approaches, including unsupervised machine learning, seismic array analysis, and stochastic modeling of seismicity generation and evolution.

Aldo Zollo was born on November 9, 1959, in Naples, Italy. He received the physics degree in 1983, and the Ph.D. degree in solid Earth geophysics from the University of Paris VII, France, in 1990.

He is a Full Professor of seismology with the University of Naples "Federico II." He specializes in seismic wave propagation, earthquake fracture processes, volcano imaging, and seismic exploration and significantly contributed to earthquake early warning systems and seismic source modeling.

Dr. Zollo served key roles in national scientific committees and institutions, including INGV and ISTerre. In 2007, he received the title "Commendatore della Repubblica Italiana," and in 2020 joined the European Academy of Sciences. Currently, he leads the Seismological Laboratory (RISSC-Lab), which participates in major international research projects and operates the Irpinia Seismic Network (ISNet).

Antonella Orefice received the degree in physics from the University of Naples Federico II, Naples, Italy, in 2008, and the Ph.D. degree in geophysics from the University of Bologna, Bologna, Italy, in 2012.

She works on reservoir monitoring and analysis of microseismicity in area of hydrocarbon production. She is involved in R&D project aimed at the application of seismological methodologies to study microseismic source parameters and stress field to get useful information for the creation/validation of the geomechanical model. The expected benefit is the definition of a suitable production strategy to minimize the risk of fault reactivation.

Gianluca Dell'Elce received the Graduate degree (Hons.) in geological sciences from the University of Chieti "Gabriele dAnnunzio," Chieti, Italy, in 2007.

He has a structural geology background, with a strong knowledge in remote sensing and surface geophysics. He is the Head of the Department of Geodynamics and Geophysical Monitoring, ENI, Rome, Italy. He manages a multidisciplinary group that has the purpose of monitoring and de-risking of upstream and midstream activities. In the work group, he also manages a team developed to ensure microseismic monitoring for injection and production activities.